UDC 532.516.5:519.63
DOI: 10.15587/1729-4061.2026.361507

IDENTIFICATION OF THE INFLUENCE OF BEND ANGLE IN AN L-SHAPED CHANNEL ON INCOMPRESSIBLE VISCOUS FLOW

Almas Temirbekov
PhD*
ORCID: https://orcid.org/0000-0002-4157-2799
Zhadra Zhaksylykova
Corresponding author
PhD
Department of Mathematics
Sarsen Amanzholov East Kazakhstan University
30th Gvardeiskoi Divisii str., 34, Ust-Kamenogorsk, Republic of Kazakhstan, 070002
E-mail: zhaksylykova0507@mail.ru
ORCID: https://orcid.org/0009-0000-1566-1926
Bekdaulet Khudaibergen*
ORCID: https://orcid.org/0009-0004-3473-363X
Nurlan Temirbekov
Doctor of Physical and Mathematical Sciences
Department of Mathematical and Computer Modeling**
ORCID: https://orcid.org/0000-0001-7542-3778
*Department of Computational Sciences and Statistics**
**Al-Farabi Kazakh National University
Al-Farabi ave., 71, Almaty, Republic of Kazakhstan, 050040

The object of this study is steady two-dimensional incompressible viscous flow in L-shaped channels with different bend angles. The problem to be solved is to determine how the bend angle affects the flow pattern and hydraulic losses. Two geometries are compared: channels with 45° and 90° bends. The computations are carried out for Re = 500, 1000, and 2000. The flow is described by the stationary Navier-Stokes equations, which are solved by the finite element method. Newton's method is used to solve the nonlinear system. The comparison is performed under the same boundary conditions and computational parameters.

The results are analyzed using velocity and pressure fields, stream-function distributions, pressure drop, loss coefficient, and Euler number. The calculations show that the 90° bend causes a stronger change in the flow after the corner than the 45° bend. In the 90° channel, the direction of motion changes more sharply. Therefore, the velocity field downstream of the bend is more distorted, the gradients are higher, and recirculation zones become more visible as Re increases. In the 45° channel, the turn is smoother, so the velocity and pressure fields change more regularly.

The integral characteristics confirm this result. For all Re considered, the 90° bend gives a larger pressure drop than the 45° bend. The loss coefficient and Euler number vary with Re, but the 90° geometry remains less favorable. This is explained by stronger rearrangement of the flow caused by the sharper turn. The influence of the bend angle is shown both by field plots and by pressure-loss indicators. The results may be used in design of ducts, cooling channels, and pipelines when pressure losses in curved parts should be reduced

Keywords: Viscous flow, L-shaped channel, incompressible Navier-Stokes equations, finite element method

Received 16.03.2025
Received in revised form 25.05.2026
Accepted 05.06.2026
Published 29.06.2026

How to Cite: *Temirbekov, A., Zhaksylykova, Z., Khudaibergen, B., Temirbekov, N. (2026). Identification of the influence of bend angle in an L-shaped channel on incompressible viscous flow. Eastern-European Journal of Enterprise Technologies, 3 (7 (141)), 58–70. https://doi.org/10.15587/1729-4061.2026.361507*

1. Introduction

Channels with bends are used in many engineering devices, including pipe systems, ventilation ducts, and cooling channels. When the flow passes through a turn, the geometry affects the velocity distribution, the pressure drop, and the possible appearance of recirculation zones. For incompressible viscous fluids, these processes are usually modeled by the Navier-Stokes equations. The equations consist of the momentum balance and the incompressibility condition. Since exact solutions are available only for simple cases, numerical methods are needed for most channel-flow problems.

Here it is possible to use the steady Navier-Stokes model. This formulation is appropriate when the flow is treated as time-independent or when the established flow regime is of primary interest. The steady problem is simpler than the full time-dependent problem, but it is still nonlinear because of the convective term. The effect of this term becomes stronger at larger Reynolds numbers.

For a finite element approximation of incompressible flow, the velocity and pressure spaces must be chosen carefully. Some pairs of spaces can lead to unstable pressure approximations. This issue is related to the inf-sup, or Ladyzhenskaya-Babuška-Brezzi, condition. In this work, Taylor-Hood elements are used. The velocity is approximated by quadratic functions, and the pressure is approximated by linear functions.

The finite element method is suitable for the present problem because the channel geometry is not rectangular. The Navier-Stokes equations are written in weak form, and then the unknown velocity and pressure are approximated in finite-dimensional spaces. This procedure gives a nonlinear algebraic system. In the computations below, this system is solved by Newton's method.

The numerical implementation is done in FEniCS. In this environment, the weak formulation can be written in a form close to the mathematical notation, while the assembly of the finite element matrices is performed automatically. This makes it convenient to test different channel geometries and boundary conditions.

Therefore, the studies of incompressible viscous flow in channels with bends is relevant for engineering flow systems. The bend angle can change the velocity distribution, pressure drop, and formation of recirculation zones. These effects are important when estimating hydraulic losses in pipe systems, ventilation ducts, and cooling channels.

2. Literature review and problem statement

The finite element method is widely used for nonlinear and incompressible flow problems. The work [1] considers numerical methods for nonlinear variational problems and is useful because the finite element discretization of the stationary Navier-Stokes equations leads to a nonlinear algebraic problem. However, this work does not study the influence of channel geometry on hydraulic losses. In [2], a finite element approximation of the stationary Navier-Stokes equations is analyzed, including stability, convergence, and error estimates for velocity and pressure. This source gives a mathematical basis for the present numerical method, but it does not consider bent channels or pressure losses caused by a change in geometry. The paper [3] presents finite element modeling using FEniCSx and parallel processing. Its main value for the present work is computational, but it does not analyze the flow in L-shaped channels. The books [4] and [5] describe the theory and implementation of the finite element method. They are useful for the weak formulation and finite element approximation, but they do not study the physical effect of a 45° or 90° bend.

Thus, the works [1–5] justify the use of FEM for nonlinear flow problems. However, their aim is mainly mathematical or computational. They do not answer the engineering question considered in this paper: how the bend angle affects the velocity field, pressure distribution, recirculation zone, and hydraulic losses.

The influence of bends on flow structure and losses has been studied in several experimental and numerical works. In [6], experimental and CFD studies showed that the bend shape of a pipeline channel affects wall damage. In particular, a 45° bend caused less damage than a 90° bend. This result confirms the importance of bend geometry. However, the main quantity studied in [6] is wall damage, not the pressure field, stream function, Euler number, or recirculation zones in a two-dimensional L-shaped channel. In [7], flow after an angled pipe bend was studied using laser velocity measurements. The authors analyzed Dean vortices and showed that a pipe bend can produce complex three-dimensional flow. This work is important physically, but it deals with turbulent three-dimensional pipe flow, while the present paper considers a stationary two-dimensional model.

The works [8] and [9] are closer to the present problem because they consider two-dimensional miter bends. In [8], flow in a two-dimensional constant-width 90° miter bend was studied, and it was shown that the sharp bend strongly affects the downstream mean flow. However, only the 90° bend was considered, so the influence of the bend angle was not studied by comparison with a 45° geometry. In [9], fluid flow and heat transfer in a two-dimensional miter bend were analyzed. The authors compared pressure losses, velocity distributions, streaklines, and numerical results. This work is close to the present study because the Reynolds numbers were of the order of 2000. However, it also does not give a direct comparison of 45° and 90° L-shaped channels under the same boundary conditions.

In [10], pressure-driven flow in microchannels with miter bends was studied experimentally. The authors showed that bends can lead to additional pressure losses and vortex formation. However, the geometry and scale of the problem are different from the present two-dimensional L-shaped channel. In [11], the pressure-loss coefficient of 90° sharp-angled miter elbows was measured for a wide range of Reynolds numbers. This work is useful for comparison of pressure losses, but it is limited to 90° miter elbows and does not compare 45° and 90° channels. In [12], head losses and loss coefficients were studied experimentally for 45° and 90° PVC pipe elbows. This work confirms that the bend angle affects local hydraulic losses. However, it considers pipe elbows and a different Reynolds-number range, so its results cannot be directly transferred to the present two-dimensional model.

Therefore, the works [6–12] show that bends can change the velocity distribution, produce recirculation zones, and increase pressure losses. At the same time, they leave part of the problem unexplored. Most of them consider pipe elbows, ducts, microchannels, turbulent regimes, or only 90° bends. This is mainly due to the fact that experimental works are usually connected with real engineering pipe systems, where three-dimensional effects and secondary flows are important. As a result, there is still a need for a separate two-dimensional comparison of 45° and 90° L-shaped channels under the same computational conditions.

Other works are focused on numerical methods for complex domains. In [13], stationary incompressible flow around a cylinder was modeled using FEM, FEniCS, and Gmsh. The results agreed with the DFG 2D-1 benchmark values, which shows that FEniCS can be used for laminar incompressible flow problems. However, this is a benchmark problem and not a comparison of bent channels. The paper [14] considers a numerical algorithm for the Navier-Stokes equations and its CUDA implementation. This work is relevant for computational efficiency, but it does not study the influence of bend angle. In [15], the Navier-Stokes equations in doubly connected domains were studied using the fictitious-domain method. In [16], a related fictitious-domain approach was applied to problems with complex curvilinear boundaries. In [17], a modified fictitious-domain method with Brinkman penalization was considered for unsteady Navier-Stokes equations. These works are important for treating complex domains, but their main aim is the numerical method, not the hydraulic comparison of 45° and 90° bends. In [18], a coordinate transformation method was used for Navier-Stokes equations in stream-function and vorticity variables. This work shows another way to work with complex geometry, but it does not analyze pressure losses in L-shaped channels.

Thus, the works [13–18] show that complex flow domains can be treated by different numerical approaches. However, they do not study the particular geometric question considered here: how the bend angle changes recirculation and hydraulic losses when all other computational conditions are the same. This is because these works are mainly focused on numerical methods for complex domains, benchmark computations, or computational efficiency, while the comparison of hydraulic losses for different bend angles is outside their main purpose.

The stationary Navier-Stokes model is suitable for many engineering problems where an established flow regime is considered. The book [19] describes the physical basis of pressure losses, flow separation, recirculation, and the role of the Reynolds number. However, it gives general physical

information and does not solve the present two-dimensional L-shaped channel problem. The book [20] gives a mathematical treatment of steady-state Navier-Stokes problems and supports the use of the stationary incompressible model. However, it does not compare different channel geometries. Taylor-Hood finite elements are a common stable choice for incompressible flow problems. The source [21] describes finite element methods and automated solution of differential equations, including tools used in FEniCS. The works [22–24] describe numerical methods, the FEniCS project, and tutorial aspects of solving partial differential equations in Python with FEniCS. These works are useful for implementation, but they do not analyze the physical influence of bend angle. The paper [25] gives an example of FEniCSx implementation for a heat conduction problem, but it is not devoted to Navier-Stokes flow. The paper [26] describes Gmsh as a mesh generator, which is relevant for building meshes in the present work. The paper [27] uses Newton's method for a nonlinear algebraic system, which is relevant because the stationary Navier-Stokes equations also require a nonlinear solver. However, [25–27] mainly support the computational tools and do not study the flow in bent channels. These sources are used mainly to justify the mathematical model, finite element approximation, software tools, mesh generation, and nonlinear solver; therefore, they do not address the physical influence of the bend angle.

The analysis of the cited works allows the unresolved part of the problem to be stated as follows. The finite element method, the stationary Navier-Stokes model, FEniCS implementation, mesh generation, and nonlinear solvers are well developed. Also, many studies show that bends and elbows influence flow structure and pressure losses. However, the available works do not give a direct comparison of steady two-dimensional incompressible flow in L-shaped channels with 45° and 90° bends under the same Reynolds numbers, boundary conditions, and numerical method. In particular, it remains necessary to compare the velocity field, pressure field, stream function, recirculation zone, pressure drop, hydraulic loss coefficient, and Euler number for these two geometries.

All this allows to assert that it is expedient to conduct a study on the influence of bend angle on incompressible viscous flow in L-shaped channels is relevant for estimating pressure losses and recirculation zones in engineering flow systems.

3. The aim and objectives of the study

The aim of the study is to identify the influence of the bend angle on steady incompressible viscous flow in L-shaped channels using the finite element solution of the stationary Navier-Stokes equations in velocity-pressure variables. This will allow estimating which channel geometry gives smaller recirculation zones and lower pressure losses in engineering flow systems.

To achieve this aim, the following objectives were accomplished:

– to obtain the velocity fields for L-shaped channels with bend angles of 90° and 45° at the considered Reynolds numbers;

– to obtain the pressure fields for both channel geometries at the considered Reynolds numbers;

– to compute the stream-function fields for both channel geometries in order to show the recirculation zones;

– to calculate the pressure drop, hydraulic loss coefficient, and Euler number for both channel geometries.

4. Materials and methods

The object of the study is steady two-dimensional incompressible viscous flow in L-shaped channels with different bend angles. The main hypothesis of the study is that the bend angle affects the velocity field, pressure field, recirculation zone, and hydraulic losses. It is assumed that the fluid is Newtonian and incompressible, and that the flow regime can be described by the stationary Navier-Stokes equations. These simplifications make it possible to compare the influence of the channel geometry under the same numerical conditions.

The physical formulation of the problem consists of studying the hydrodynamics of pipeline channels. In modern plumbing, channels with a 45° angle are commonly used. They provide smoother water flow, reduce pressure losses, and lower the risk of blockages compared to sharp 90° bends. This work considers two types of L-shaped channels (Fig. 1).

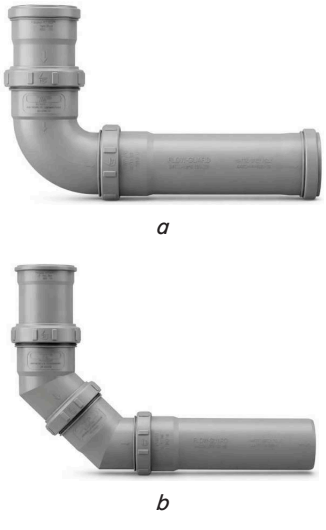

Fig. 1. L-shaped channels: *a* – channel with a 90° bend; *b* – channel with a 45° bend

As shown in Fig. 2, *a*, the channel has a sharp 90° bend in the first configuration. Despite its simplicity, this geometry leads to an abrupt change in flow direction in the bend region, which causes the formation of intense vortices and significant pressure losses.

In the second configuration, shown in Fig. 2, *b*, the turn is achieved not through a single sharp bend, but through two successive 45° bends. This approach is widely used in modern plumbing and engineering practice, as the gradual change in flow direction reduces vortex intensity and decreases the hydraulic resistance of the system.

To study this type of problem using numerical schemes, let's consider a simplified planar case. Let's consider steady-state Navier-Stokes problem in a two-dimensional domain $\Omega \subset R^2$:

$$\begin{cases} -\frac{1}{\mathrm{Re}}\nabla^2\mathbf{u} + (\mathbf{u}\cdot\nabla)\mathbf{u} + \nabla p = 0, & \mathbf{x} \in \Omega, \\ \nabla\cdot\mathbf{u} = 0, & \mathbf{x} \in \partial\Omega, \end{cases} \quad (1)$$

where the first term in the left-hand side of the first equation is the viscous term, $(\mathbf{u}\cdot\nabla)\cdot\mathbf{u}$ – the convective term, ∇p – the pressure gradient, Re – the Reynolds number, and the domain Ω has the shape of a curved channel. The problem involves determining two fields, namely, the velocity field $\mathbf{u} = (u_1, u_2)$: $\Omega \to R^2$, a vector field describing the

fluid pressure at each point of the domain, and the pressure fields, $p : \Omega \to \mathrm{R}$, a scalar field describing the fluid pressure at each point of the domain.

A two-dimensional pipeline channel with complex geometry is considered as the computational domain shown in Fig. 2. The domain is divided into three subdomains: Ω_1, Ω_2, and Ω_3:

$$\Omega_1 = \left\{x_{\min} \le x_1 \le x_{\max}, x_{\max} \le x_2 \le L_2\right\},$$

$$\Omega_2 = \left\{x_{\min} \le x_1 \le x_{\max}, x_{\max} \le x_2 \le f\left(x_1\right)\right\},$$

$$\Omega_3 = \left\{x_{\max} \le x_1 \le L_1, x_{\min} \le x_2 \le x_{\max}\right\},$$

where $x_2 = f(x_1)$ – a function describing the lower rigid boundary of Γ_ω for $x_{\min} \le x_1 \le x_{\max}$.

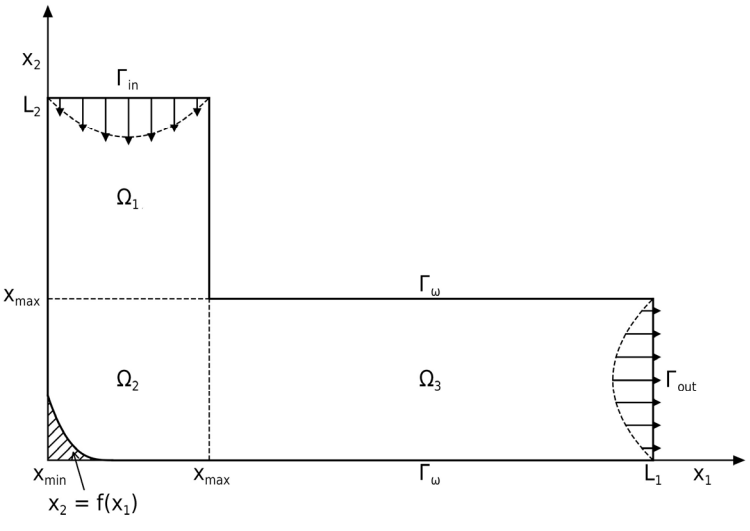

Fig. 2. Geometric diagram of the calculation area of the pipeline channel

The boundary of the computational domain consists of three parts

$$\partial\Omega = \Gamma_{in} \cup \Gamma_{out} \cup \Gamma_{\omega},$$

where Γ_{in} – the inlet boundary

$$\Gamma_{in} = \left\{x_2 = L_2, x_{\min} \le x_1 \le x_{\max}\right\},$$

Γ_{out} – the outlet boundary

$$\Gamma_{out} = \left\{x_1 = L_1, x_{\min} \le x_2 \le x_{out}\right\}.$$

and Γ_ω – the solid walls.

At the inlet boundary Γ_{in}, the velocity is prescribed. The flow enters with a downward-directed parabolic profile:

$$\mathbf{u} = \mathbf{u}_{in}\left(\mathbf{x}\right), \ \ \mathbf{x} \in \Gamma_{in},$$

$$u_1 = 0, \quad u_2 = -U_{\max} \cdot \frac{4\left(x_1 - x_{\min}\right)\left(x_{\max} - x_1\right)}{D^2}, \tag{2}$$

where $D = x_{\max} - x_{\min}$ is the width of the inlet cross-section, $U_{\max}$ – the maximum velocity at the center.

Let's consider Dirichlet boundary condition on the walls Γ_ω (no-slip)

$$\mathbf{u} = 0, \quad \mathbf{x} \in \Gamma_{\omega}, \tag{3}$$

which means that the fluid at a solid wall remains stationary, and natural boundary condition at the outlet

$$\mathbf{v}\frac{\partial \mathbf{u}}{\partial n} - pn = 0, \quad \mathbf{x} \in \Gamma_{out}. \tag{4}$$

When numerically solving the posed steady-state problem (1)–(4) in a curved domain, one of the unresolved issues is modeling the vertical inlet and horizontal outlet flows depending on the bending angle. This study examines the dynamics of velocity and pressure field changes depending on the input parameters and flow boundary conditions. The choice of domain geometry is considered optimal if the recirculation zones in the bending zone are reduced. Problem (1)–(4) is solved in terms of velocity-pressure variables, and to study the size of the recirculation zone, it is necessary to determine the stream function field. Based on the numerical results obtained, determining the stream function in curved domains is a separate problem. Various methods exist; in this paper, the stream function is found by introducing a velocity vortex, which leads to the solution of an elliptic equation for the stream function, on the right-hand side of which is the velocity vorticity.

4. 1. FEniCS package

FEniCS is an open-source package that uses FEM to solve PDEs by turning scientific models into effectual finite element code. FEniCS is easy to get started with and also offers more advanced capabilities for more knowledgeable users [16–18]. FEniCS requires the PDE to be expressed in the variational or weak form [19, 20]. The variational problem is entered into Python using the Unified Field Language (UFL). The geometry and mesh are created using Gmsh [21].

4. 2. Variational formulation

Let's introduce functional spaces for the trial and test speed functions:

$$V_g = \left\{\mathbf{v} \in \left[H^1\left(\Omega\right)\right]^2 : \mathbf{v}\big|_{\Gamma_{in}} = \mathbf{u}_{in}, \ \mathbf{v}\big|_{\Gamma_{\omega}} = 0\right\}, \tag{5}$$

$$V_0 = \left\{\mathbf{v} \in \left[H^1\left(\Omega\right)\right]^2 : \mathbf{v}\big|_{\Gamma_{in} \cup \Gamma_{\omega}} = 0\right\},$$

and pressure

$$Q = \left\{q \in L^2\left(\Omega\right) \middle| \int_{\Omega} q \mathrm{d}\Omega = 0\right\}. \tag{6}$$

In (5), (6) and further on, the generally accepted notations from works [1, 2] are used.

Let's multiply the momentum equation (1) and the continuity equation (2) by test functions $\mathbf{v} \in V_0$ and $q \in Q$, respectively, and integrate over the domain Ω:

$$\int_{\Omega}\left(-\frac{1}{\mathrm{Re}}\nabla^2\mathbf{u} + \left(\mathbf{u}\cdot\nabla\right)\mathbf{u} + \nabla p\right)\cdot\mathbf{v}\,\mathrm{d}\Omega = 0,$$

$$\int_{\Omega}\left(\nabla\cdot\mathbf{u}\right)q\,\mathbf{d}\Omega = 0.$$

Applying integration by parts, let's obtain the variational formulation:

$$\frac{1}{\mathrm{Re}}\int_{\Omega}\nabla\mathbf{u}:\nabla\mathbf{v}\,\mathrm{d}\Omega+\int_{\Omega}\left(\mathbf{u}\cdot\nabla\right)\mathbf{u}\cdot\mathbf{v}\,\mathrm{d}\Omega-$$
$$-\int_{\omega}p\left(\nabla\cdot\mathbf{v}\right)\mathrm{d}\Omega=0, \quad (7)$$

$$\int_{\Omega}\left(\nabla\cdot\mathbf{u}\right)q\,\mathrm{d}\Omega=0. \quad (8)$$

Now let's present the expansion of the solution in terms of basis functions of the second order $\phi_i(x)$, $i = 1, ..., N_u$ and the first order $\phi_j(x)$, $j = 1, ..., N_p$. The unknown functions are expressed in terms of basis functions are follows

$$\mathbf{u}_h\left(\mathbf{x}\right)=\sum_{i=1}^{N_u}U_i\phi_i\left(\mathbf{x}\right),\ p_h\left(x\right)=\sum_{j=0}^{N_p}P_j\psi_j\left(x\right).$$

According to the Galerkin method, trial functions are selected from the same basis functions

$$\mathbf{v}_h=\phi_k,\ k=1,\ldots,N_u,\ q_h=\psi_l,\ l=1,\ldots,N_p. \quad (9)$$

Substitution of (9) into the variational form (7), (8) gives:

$$\frac{1}{\mathrm{Re}}\sum_{i=1}^{N_u}U_i\int_{\Omega}\nabla\phi_i:\nabla\phi_k\mathrm{d}\Omega+$$
$$+\sum_{i=1}^{N_u}\sum_{j=1}^{N_u}U_iU_j\int_{\Omega}\left(\phi_j\cdot\nabla\right)\phi_i\cdot\phi_k\,\mathrm{d}\Omega-$$
$$-\sum_{j=1}^{N_p}P_j\int_{\Omega}\psi_j\left(\nabla\cdot\phi_k\right)\mathrm{d}\Omega=0, \quad (10)$$

$$\sum_{i=1}^{N_u}U_i\int_{\Omega}\left(\nabla\cdot\phi_i\right)\psi_l\,\mathrm{d}\Omega=0. \quad (11)$$

After the transformations, (10), (11) take the form of a block system

$$\begin{pmatrix}A+\mathbf{N}\left(\mathbf{U}\right) & B\\ B^T & 0\end{pmatrix}\begin{pmatrix}\mathbf{U}\\ \mathbf{P}\end{pmatrix}=\begin{pmatrix}0\\ 0\end{pmatrix}, \quad (12)$$

where:

$$A_{ki}=\frac{1}{\mathrm{Re}}\int_{\Omega}\nabla\phi_i:\nabla\phi_k\,\mathrm{d}\Omega,$$

$$B_{li}^T=\int_{\Omega}\left(\nabla\cdot\phi_i\right)\psi_l\,\mathrm{d}\Omega,$$

$$B_{kj}=-\int_{\Omega}\psi_j\left(\nabla\cdot\phi_k\right)\mathrm{d}\Omega,$$

$$C_k\left(\mathbf{U}\right)=\sum_{i,j}U_iU_j\int_{\Omega}\left(\phi_j\cdot\nabla\right)\phi_i\cdot\phi_k\,\mathrm{d}\Omega,$$

and $\mathbf{N}(\mathbf{U})$ – the nonlinear convection matrix, $\mathbf{U}$ – the vector of unknown velocities, $\mathbf{P}$ – the vector of the unknown pressure.

4. 3. Newton's method for the approximate solution of the system (12)

Let's introduce the vector-valued function $\mathbf{F}: R^{n+m}\to R^{n+m}$, and rewrite the system (12) as follows

$$\mathbf{F}\left(\mathbf{U},\mathbf{P}\right)=\begin{pmatrix}\left(A+\mathbf{N}\left(\mathbf{U}\right)\right)\mathbf{U}+B\mathbf{P}\\ B^T\mathbf{U}\end{pmatrix}=\begin{pmatrix}0\\ 0\end{pmatrix}.$$

The Jacobian of the system is $J = D\mathbf{F}$. Let's differentiate with respect to ($\mathbf{U}$, $\mathbf{P}$). The nonlinearity appears only in the upper block

$$\frac{\partial}{\partial\mathbf{U}}\left(\mathbf{N}\left(\mathbf{U}\right)\mathbf{U}\right)=\mathbf{N}\left(\mathbf{U}\right)+D\mathbf{N}\left(\mathbf{U}\right)\cdot\mathbf{U},$$

where $D\mathbf{N}(\mathbf{U})\cdot\mathbf{U}$ – the Fréchet derivative of the convective term. In matrix element form

$$\left(D\mathbf{N}\left(\mathbf{U}\right)\cdot\mathbf{U}\right)_{ki}=\sum_j\mathbf{U}_j\int_{\Omega}\left(\phi_j\cdot\nabla\right)\phi_i\cdot\phi_k\,\mathrm{d}\Omega+$$
$$+\sum_j\mathbf{U}_j\int_{\Omega}\left(\phi_i\cdot\nabla\right)\phi_j\cdot\phi_k\,\mathrm{d}\Omega.$$

Thus the full Jacobian takes the form:

$$J\left(\mathbf{U}^n,\mathbf{P}^n\right)=\begin{pmatrix}A+\mathbf{N}\left(\mathbf{U}^n\right)+D\mathbf{N}\left(\mathbf{U}^n\right)\cdot\mathbf{U}^n & B\\ B^T & 0\end{pmatrix}.$$

At each iteration $n = 0, 1, 2, ...$, let's solve the linear block system

$$J\left(\mathbf{U}^n,\mathbf{P}^n\right)\begin{pmatrix}\delta\mathbf{U}\\ \delta\mathbf{P}\end{pmatrix}=-\mathbf{F}\left(\mathbf{U}^n,\mathbf{P}^n\right),$$

then, let's update the solution by formulas

$$\mathbf{U}^{n+1}=\mathbf{U}^n+\delta\mathbf{U},\ \mathbf{P}^{n+1}=\mathbf{P}^n+\delta\mathbf{P},$$

until the stopping criterion is satisfied

$$\left\|\mathbf{F}\left(\mathbf{U}^n,\mathbf{P}^n\right)\right\|\le\varepsilon\left\|\mathbf{F}\left(\mathbf{U}^0,\mathbf{P}^0\right)\right\|.$$

Newton's method exhibits quadratic convergence in the vicinity of the solution

$$\left\|e^{n+1}\right\|\le C\left\|e^n\right\|^2,$$

where $e^n = (U^n, P^n) - (U^*, P^*)$ – the error of the n-th step, and (U^*, P^*) – the exact solution.

The accuracy of the numerical calculations was controlled for the discrete nonlinear system obtained after finite element discretization of the stationary Navier-Stokes equations. For each Reynolds number and each channel geometry, Newton's method was applied with the same stopping criteria. The iterations were stopped when the residual norm became less than 10^{-8}, and the norm of the difference between two consecutive Newton iterates became less than 10^{-10}. These two criteria were used together to check that the algebraic system was solved with sufficient accuracy and that the computed solution no longer changed noticeably. The linear systems arising at Newton iterations were solved with the same solver settings in all calculations. Thus, the same accuracy requirements were used for both bend angles and all Reynolds numbers. Therefore, all velocity and pressure fields, pressure drops, loss coefficients, and Euler numbers were obtained under the same nonlinear solver accuracy conditions.

The stream function $\psi(x, y)$ is determined by the velocity field $\mathbf{u} = (u_x, u_y)$. In the two-dimensional case, the following relationship is used

$$u_1=\frac{\partial\psi}{\partial x_2},\quad u_2=-\frac{\partial\psi}{\partial x_1}. \quad (13)$$

Vorticity is defined as

$$\omega = \frac{\partial u_2}{\partial x_1} - \frac{\partial u_1}{\partial x_2}.$$

Then the stream function is found from the solution of the Poisson problem

$$-\Delta\psi = \omega,$$

where Δ – the Laplace operator. The corresponding weak formulation is written as

$$\int_\Omega \nabla\psi \cdot \nabla\phi \mathrm{d}x = \int_\Omega \omega\phi \mathrm{d}x,$$

and the following boundary conditions are imposed.

The boundary condition for the stream function can be determined from the input boundary condition (2), using the second formula (13). Then the stream function at the input boundary:

$$\psi(\xi, L_2) = \frac{U_{\max}}{D^2}\begin{bmatrix} -\frac{1}{3}\left(\xi^3 - x_{\min}^3\right) + \\ +\frac{1}{2}\left(x_{\max} + x_{\min}\right)\left(\xi^2 - x_{\min}^2\right) + \\ +x_{\min}x_{\max}\left(\xi - x_{\min}\right) \end{bmatrix},$$

$$x_{\min} \le \xi \le x_{\max}.$$

Therefore, the stream function on the lower boundary $\Gamma_{\omega lower}$ that is, at $\xi = x_{\min} = 0$ is $\psi_{\omega lowe}r = 0$, while on the upper solid wall $\Gamma_{\omega upper}$, that is, at $\xi = x_{\max}$ is

$$\psi_{\omega upper} = \frac{1}{6}\frac{U_{\max}}{D^2}x_{\max}^3.$$

A "soft" boundary condition can be imposed on the outlet boundary Γ_{out}

$$\left.\frac{\partial\psi}{\partial x_1}\right|_{x=\Gamma_{out}} = 0.$$

Thus, the described method gives the numerical procedure used in this work. First, the stationary Navier-Stokes problem is written in weak form. Then it is discretized by the finite element method and solved by Newton's method. The computed velocity and pressure fields are used further to analyze the flow pattern, recirculation zones, pressure drop, loss coefficient, and Euler number.

5. Numerical results of modeling the flow in bended channels

5. 1. The velocity field

Fig. 3 presents the velocity vector field of fluid flow in an L-shaped channel. The field is represented by arrows (vectors), each indicating the local direction of fluid motion at the corresponding point in the domain.

The arrow directions illustrate the flow trajectory and allow visualization of changes in the flow pattern, particularly in the bend region of the channel.

This type of visualization provides a clear representation of the flow structure and reveals the characteristic features of fluid motion in a channel with complex geometry.

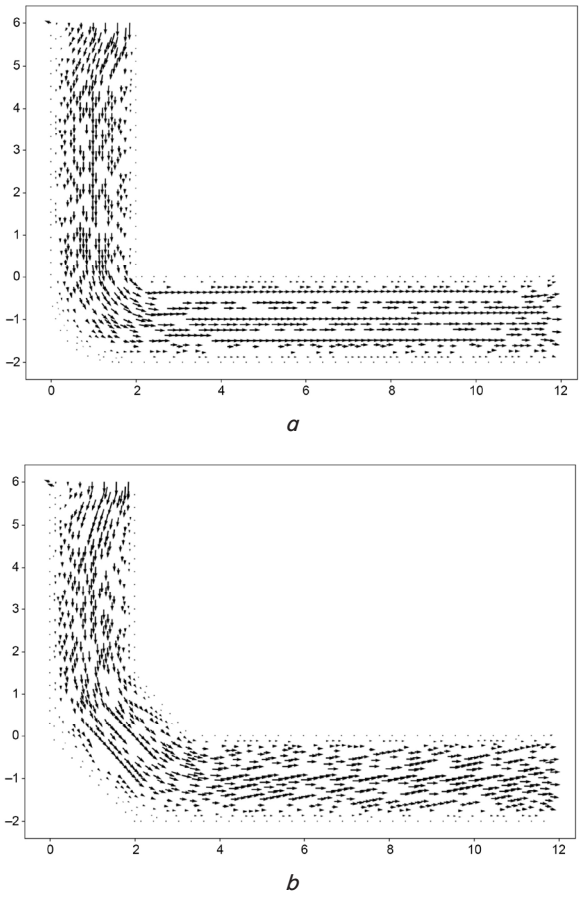

Fig. 3. Velocity field in an L-shaped channel: *a* – channel with a 90° bend; *b* – channel with a 45° bend

Fig. 4 presents the velocity contour lines of fluid flow in L-shaped channels with 90° and 45° bends. These contours illustrate the velocity distribution throughout the channel, where lines connecting points of equal velocity provide a clear visualization of the flow structure.

A noticeable increase in velocity is observed in the bend region. This is due to the fact that the flow changes direction, causing a redistribution of velocities: in certain areas the fluid accelerates, particularly closer to the inner side of the bend. At the same time, along the straight sections of the channel, the velocity gradually becomes more uniform, forming a more stable and well-defined flow profile.

When the two geometries are compared, the 45° channel gives a smoother passage of the flow through the bend. The direction of motion changes gradually, and no sharp velocity jumps are observed in the computed field. For the 90° bend, the situation is different. The flow is forced to turn over a shorter region, so the deformation of the velocity field is stronger. Higher velocity gradients appear near the bend, and local zones with more complicated motion can be seen. Therefore, the bend angle noticeably changes the flow character inside the channel.

Fig. 4 shows the velocity field in two channels with bends of 90° and 45°. In both cases, it can be seen that the velocity magnitude is largest in the central parts of the channels. Therefore, red regions appear in the central parts of the chan-

nels. On the solid walls, the no-slip condition is prescribed. There the velocity decreases and becomes zero, so blue regions appear near the channel walls.

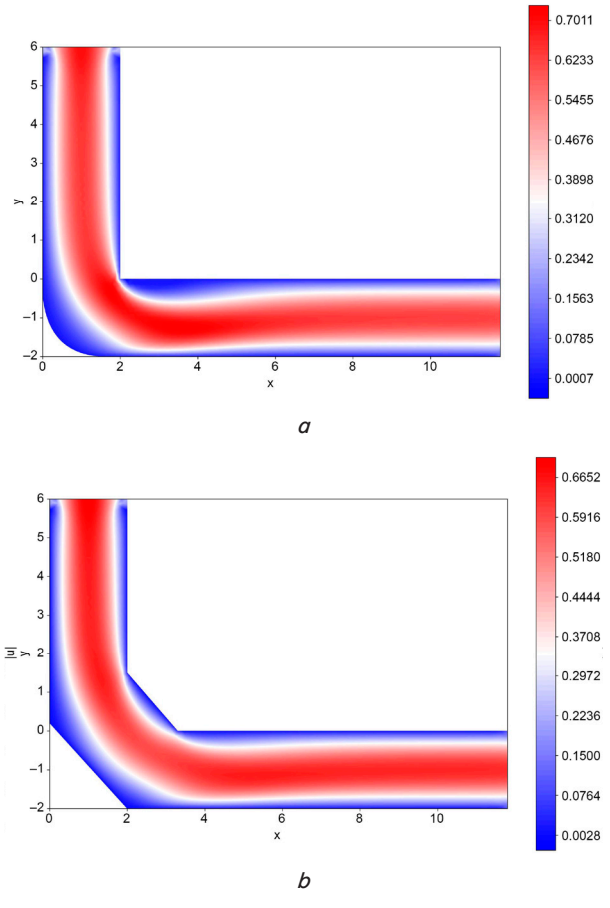

Fig. 4. Contour isolines of the velocity field distribution: *a* — channel with a 90° bend; *b* — channel with a 45° bend

It can be seen that the flow direction in the channel with the 90° bend changes more sharply. Therefore, larger velocity gradients appear in the bend region of this channel. Also, in the channel with the 90° bend, the flow directly meets the solid wall in the bend region. This can increase the possibility of blockage in practical channels.

In the channel with the 45° bend, the change in the flow direction is smoother. Therefore, the velocity field is more uniform, and the velocity changes more gradually in the bend region. The flow also becomes more stable after the turn.

Thus, the channel geometry has a visible influence on the flow structure. The 45° bend gives a smoother and more uniform flow, while the 90° bend causes a sharper change in the velocity field and flow deceleration near the corner.

5. 2. The pressure field

The pressure distribution p was computed for two channel geometries with bend angles of 45° and 90°. The obtained numerical results are shown in Fig. 5. The color scale in the figure shows the pressure values in the computational domain: red corresponds to regions with higher pressure, and blue corresponds to regions with lower pressure. This representation makes it possible to compare how the change in the channel bend angle affects the pressure distribution inside the flow domain.

Fig. 5 shows the pressure distribution in channels with different bend geometries. In both cases, a high-pressure region is observed near the inlet boundary. This region is shown in red. As the flow passes through the bend and then moves along the horizontal part of the channel, the pressure gradually decreases.

In the channel with the 90° bend, the flow direction changes rather sharply. Therefore, a clearly visible blue region appears near the inner corner. This shows that the pressure in this part drops sharply and reaches its minimum value.

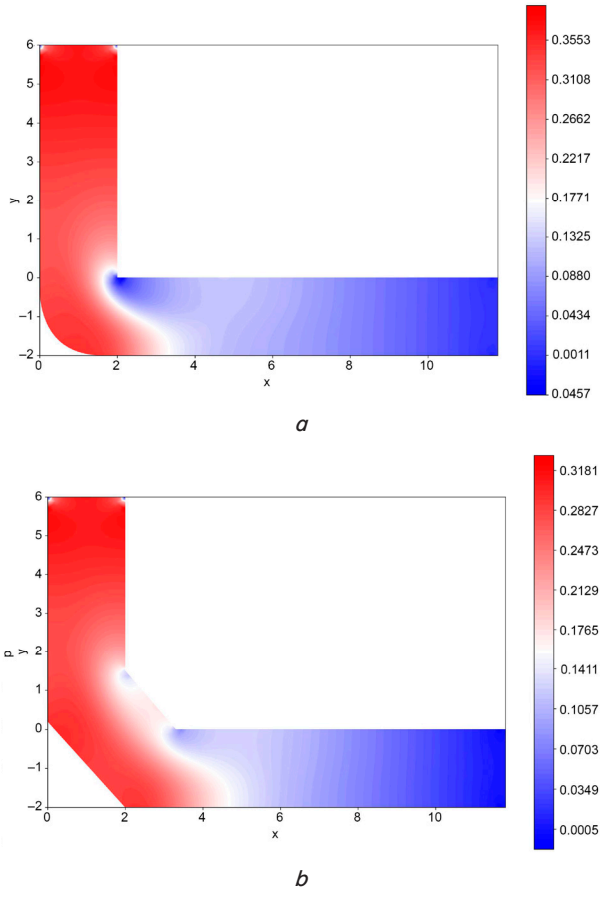

Fig. 5. Pressure field contour isolines: *a* — channel with a 90° bend; *b* — channel with a 45° bend

At the inlet part, the pressure is also high, but after the sharp bend it decreases more strongly than in the 45° channel. In the horizontal part of the channel, the pressure gradually decreases toward the outlet. Thus, the 90° bend creates a stronger disturbance of the flow and a more visible pressure drop near the corner.

In the channel with the 45° bend, the pressure changes more smoothly. A higher pressure value is observed in the vertical inlet part, so this region is shown in red. After the bend, the pressure gradually decreases. This is seen from the blue color in the horizontal part of the channel, where the pressure becomes lower as the flow moves toward the outlet.

In the bend region, a very sharp pressure drop is not observed. This shows that the 45° bend is smoother for the flow.

5. 3. Current function

Fig. 6 shows the stream function for the L-shaped channels with bend angles 45° and 90° at different Reynolds numbers. The contours of ψ represent streamlines and make it possible to examine the structure of the flow.

When the Reynolds number increases, the streamlines become more curved near the bend. Local recirculation

zones also become more visible. This is related to the growing role of inertia.

In the 90° channel, the disturbance near the turning region is stronger for all Reynolds numbers. The streamlines are compressed near the inner wall, and their clustering becomes more noticeable as Re increases. This shows that the sharper bend produces a more disturbed flow pattern.

In the 45° channel, the streamlines change direction more gradually. Even at the largest Reynolds number considered, the flow pattern remains smoother than in the 90° case, and the recirculation zones are weaker.

These results show two effects at the same time. Increasing Re strengthens inertial effects, while reducing the bend angle makes the flow more regular and decreases the intensity of vortical structures.

Fig. 6 shows the stream-function distribution ψ for channels with bend angles of 45° and 90° at Reynolds numbers Re = 500, 1000, and 2000. The stream-function lines make it possible to trace the character of fluid motion inside the channel.

For the channel with the 45° bend, the stream-function lines are distributed rather uniformly. As the Reynolds number increases from 500 to 2000, the flow keeps a smooth character. The streamlines pass through the bend region gradually and then enter the horizontal part of the channel without sharp changes. This shows that the geometry of the 45° channel provides a smoother change in the flow direction.

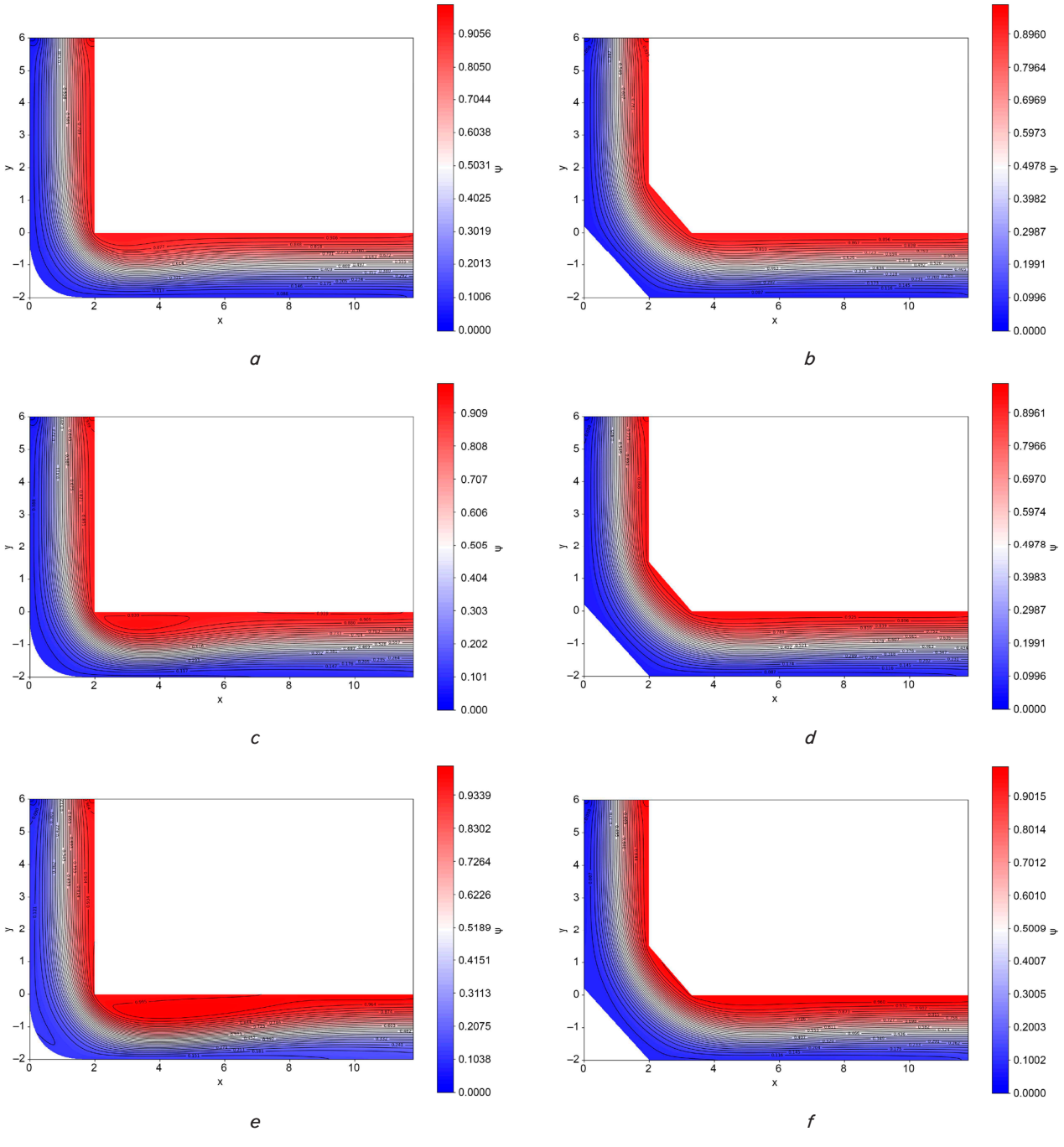

Fig. 6. Visualization of the stream function ψ in L-shaped channels for different bend angles and Reynolds numbers: *a* – channel with a 90° bend at Re = 500; *b* – channel with a 45° bend at Re = 500; *c* – channel with a 90° bend at Re = 1000; *d* – channel with a 45° bend at Re = 1000; *e* – channel with a 90° bend at Re = 2000; *f* – channel with a 45° bend at Re = 2000

In the channel with the 90° bend, the flow pattern is more complex. At Re = 500, the flow still passes through the bend in a relatively stable way, but the stream-function lines are already more strongly curved near the corner. When the Reynolds number increases to Re = 1000 and Re = 2000, local vortex zones appear after the bend. This is seen from the closed or strongly curved stream-function lines in the horizontal part of the channel. Such zones appear because of the sharp change in the flow direction near the 90° corner.

Thus, an increase in the Reynolds number strengthens the influence of channel geometry on the flow structure. In the channel with the 45° bend, the stream-function lines remain more uniform, and the flow keeps a smoother character. In the channel with the 90° bend, vortices and zones of nonuniform motion appear as Re increases, especially after the bend. This shows that the sharp 90° bend disturbs the flow more strongly than the smoother 45° bend.

5. 4. The pressure drop, hydraulic loss coefficient, and Euler number for both channel geometries

To compare the two channel geometries quantitatively, it is possible to calculate the pressure drop ΔP, the friction coefficient C_f, and the Euler number Eu for several Reynolds numbers. The computations are performed for channels with bend angles 45° and 90°.

The pressure-drop values are higher in the 90° channel for all Reynolds numbers. The reason is the sharper turn of the flow. In this geometry, the direction of motion changes over a shorter distance, so the inertial contribution near the bend becomes stronger. The pressure field is less uniform in this region, and the total hydraulic resistance increases.

At Re = 500, the pressure drop in the 90° channel is approximately 10.1% larger than in the 45° channel. At Re = 1000, the difference is about 10.8%. At Re = 2000, it reaches approximately 12.2%. The increase of this difference with Re shows that the influence of the bend geometry becomes more visible when inertial effects grow.

The same tendency is obtained for C_f and Eu. Their values are larger for the 90° channel, which means that this geometry produces higher energy losses. The agreement between the pressure drop, friction coefficient, and Euler number supports the consistency of the comparison.

As the Reynolds number grows, the absolute value of C_f decreases because viscous effects become relatively weaker. However, the difference between the two geometries remains. In the considered range of Re, the bend angle continues to be one of the main factors controlling the hydraulic losses.

The simulations therefore show that replacing the 90° bend by a 45° bend reduces the pressure drop and hydraulic resistance. The smoother turn also leads to a more regular flow distribution inside the channel.

The average pressure on a boundary segment is computed by integration over that segment:

$$p_{inlet} = \frac{\int\limits_{\Gamma_{in}} p\,ds}{\int\limits_{\Gamma_{in}} ds}, \quad p_{outlet} = \frac{\int\limits_{\Gamma_{out}} p\,ds}{\int\limits_{\Gamma_{out}} ds},$$

$$\Delta P = p_{inlet} - p_{outlet}.$$

The hydraulic loss coefficient and the Euler number are calculated as follows

$$C_f = \frac{\Delta P}{\frac{1}{2}\rho U_{\max}^2}, \quad \mathrm{Eu} = \frac{\Delta P}{\rho U_{\max}^2}.$$

The corresponding numerical values are given in Table 1.

Table 1

Comparison of hydrodynamic flow characteristics in L-shaped channels with bend angles of 45° and 90° at different Reynolds numbers

Re (dimensionless)	Bend angle (°)	ΔP (dimensionless)	C_f (dimensionless)	Eu (dimensionless)
500	45	0.260596	0.5212	0.2606
500	90	0.286797	0.5736	0.2868
1000	45	0.123542	0.2471	0.1235
1000	90	0.136875	0.2737	0.1369
2000	45	0.055111	0.1102	0.0551
2000	90	0.061812	0.1236	0.0618

Table 1 gives the values of the pressure drop ΔP, resistance coefficient C_f, and Euler number Eu for the two channel geometries. The values are presented for Re = 500, 1000, and 2000. For all considered Reynolds numbers, the values of ΔP, C_f, and Eu are higher for the channel with the 90° bend than for the channel with the 45° bend. When the Reynolds number increases from Re = 500 to Re = 2000, these quantities decrease for both geometries.

For the channel with the 45° bend, the values of the hydrodynamic characteristics are lower. This is related to the smoother passage of the flow through the bend. Therefore, the change in the direction of motion is less abrupt. As a result, the pressure drop decreases and the resistance to the flow becomes lower.

The table also shows that, when the Reynolds number increases from Re = 500 to Re = 2000, the values of ΔP, C_f, and Eu decrease for both channel geometries. This means that, in the considered range of Reynolds numbers, the relative pressure losses and resistance become smaller. However, the channel with the 90° bend remains more resistant to the flow in all cases compared with the 45° channel.

Thus, the results in the table agree with the results obtained from the velocity, pressure, and stream-function fields. The channel with the 45° bend gives a smoother and more uniform flow, while the channel with the 90° bend causes stronger flow redistribution, larger pressure losses, and higher hydrodynamic resistance.

6. Discussion of the modeling results

The obtained numerical results show that the bend angle of the channel has a significant influence on the flow structure. This is explained by the fact that the motion of the fluid is determined not only by the Reynolds number Re, but also by the geometry of the computational domain. In the considered problem, the channel geometry is given by two bend variants: 45° and 90° (Fig. 1). The mathematical statement of the problem is given by formulas (1), (2), and the boundary conditions are given by formulas (3), (4).

From the analysis of the velocity fields in Fig. 4, it can be seen that, in the channel with the 45° bend, the flow changes

direction more smoothly. The maximum velocity values are located mainly in the central part of the channel, while near the walls the velocity decreases. This is related to the no-slip condition prescribed on the solid boundaries. In the channel with the 90° bend, the flow has to change its direction sharply. Therefore, a more visible redistribution of velocity is observed in the bend region. After the bend, the velocity field becomes less uniform than in the 45° channel.

The pressure distribution p, shown in Fig. 5, also confirms the influence of the channel shape on the flow. In both cases, higher pressure is observed in the inlet part of the channel, and the pressure decreases toward the outlet. However, in the channel with the 90° bend, the pressure changes more sharply, especially near the inner corner. This is explained by the sharp change in the direction of the flow. In the channel with the 45° bend, the pressure changes more smoothly because the turn is less sharp and the flow passes through it more evenly.

The difference between the two geometries is especially clear in the analysis of the stream function ψ for Reynolds numbers Re = 500, 1000, and 2000 (Fig. 6). In the channel with the 45° bend, the stream-function lines are distributed rather uniformly for all considered values of Re. As the Reynolds number increases, the flow becomes more intensive, but the general flow structure remains smooth. This shows that the 45° bend gives a softer change in the direction of fluid motion and does not lead to a strong formation of vortex zones.

A different pattern is observed in the channel with the 90° bend. At Re = 500, the flow still passes through the bend in a relatively stable way. However, when the Reynolds number increases to Re = 1000 and Re = 2000, vortex zones begin to appear after the bend. This can be seen from the closed or strongly curved stream-function lines in Fig. 6, *c*, *e*. The appearance of such zones is related to the fact that the flow cannot smoothly follow the sharp 90° turn. Therefore, as Re increases, the influence of the channel geometry becomes stronger, and the flow becomes more complex.

The calculated integral characteristics also confirm the influence of the bend angle. For all considered Reynolds numbers, the pressure drop in the 90° channel is larger than in the 45° channel. The loss coefficient and Euler number also show that the 90° bend is less favorable. This is caused by a sharper change in the flow direction and stronger rearrangement of the velocity field after the bend.

These results are consistent with known studies of flows in bends and elbows. A direct comparison with experimental data is limited, because the present paper considers a two-dimensional L-shaped channel, while many experimental works deal with pipe elbows, duct bends, or microchannels. Therefore, the comparison is mainly qualitative.

The stronger deformation of the velocity field in the 90° channel agrees with the results [8], where a sharp 90° miter bend was shown to strongly affect the downstream mean flow. A similar tendency was reported [9] for a two-dimensional miter bend. In the present work, this effect becomes more visible as Re increases: at Re = 500 the flow remains relatively regular, while at Re = 1000 and Re = 2000 the stream-function lines become more curved and recirculation zones appear after the 90° bend.

The formation of recirculation zones and the increase in pressure losses are also consistent with the results [10], which showed that miter bends can produce vortices and additional pressure drop in microchannels. Although their geometry is different, the same general tendency is observed here: a sharp change in flow direction makes the flow pattern more complicated and increases hydraulic losses.

The pressure-loss results also agree qualitatively with experimental data for miter elbows and pipe elbows. The paper [11] showed that the pressure-loss coefficient of 90° miter elbows depends on the Reynolds number. In the present work, the loss coefficient and Euler number also change with Re. The comparison of the 45° and 90° channels is also consistent with [12], where experimental data for pipe elbows showed that the bend angle affects local losses. In the present calculations, the 90° bend gives larger losses than the 45° bend.

Thus, the comparison with previous studies supports the main conclusion of this work: a sharper bend leads to stronger deformation of the velocity field, possible recirculation after the bend, and larger pressure losses. The 45° bend gives a smoother change in the flow direction and smaller hydraulic losses.

A feature of the presented numerical comparison is that the same mathematical model, numerical method, boundary conditions, and Reynolds numbers are used for both geometries. This makes the comparison more correct, because the difference between the obtained results is mainly related to the bend angle. Thus, the influence of the channel geometry can be separated from the influence of changes in numerical parameters.

At the same time, the comparison with other authors has limitations. The cited works do not use exactly the same geometry and boundary conditions as the present paper. Works [8, 9] are close to the present study because they consider two-dimensional miter bends, but they do not give the same comparison of 45° and 90° L-shaped channels. Work [10] considers microchannels. Works [11] and [12] consider pipe elbows. Therefore, the comparison with these studies should be understood mainly as qualitative. It supports the obtained numerical results, but it does not replace direct experimental validation for the same two-dimensional L-shaped geometry.

The internal limitations of this study are related to the chosen problem statement. The study is limited to a two-dimensional model. The influence of wall roughness, heat transfer, pipe elasticity, and three-dimensional effects is not considered. These simplifications make it possible to compare the influence of the channel geometry under the same numerical conditions, but they also limit the direct transfer of the results to real engineering systems. First, the computations were performed only for Reynolds numbers Re = 500, 1000, and 2000. Therefore, the obtained conclusions are mainly valid for this range of values. Second, only two channel geometries were considered: channels with bends of 45° and 90°. Other bend angles, smooth curvilinear turns, and more complex channel shapes were not analyzed in this work. In addition, the results depend on the selected mesh, boundary conditions, and computational parameters given in Table 1.

These limitations define the area of applicability of the obtained results. The presented conclusions can be used for the analysis of two-dimensional laminar flow in channels with similar geometry, close boundary conditions, and the considered range of Reynolds numbers. If Re is increased significantly, if the channel shape is changed, or if a three-dimensional model is used, additional checks of stability and reproducibility are needed.

The limitations of this work include the small number of considered geometric configurations. The paper analyzes only two bend angles, 45° and 90°. This limitation can be removed in future studies by considering additional angles, for example 30°, 60°, and 120°, as well as channels with a smooth curvilinear bend. Another limitation is the absence of direct experimental data for exactly the same two-dimensional L-shaped geometry. In future studies, this can be addressed by comparing the numerical results with laboratory measurements for the same geometry or with more suitable benchmark problems.

Further development of the study may be related to extending the range of Reynolds numbers, using more complex channel geometries, and moving to three-dimensional computations. It is also useful to study the influence of the mesh size, inlet velocity profile, and outlet length on the formation of vortices after the bend. At the same time, additional difficulties may appear. They may be related to the stability of the numerical method, the quality of the mesh, and the increase in computational cost. Thus, the comparison with previous studies shows that the obtained tendencies agree with known behavior of flows in bends and elbows. Direct experimental validation for the same two-dimensional geometry remains a task for future work.

7. Conclusion

1. Numerical modeling of flow in channels with different bend geometries was performed. The obtained velocity fields showed that, in the channel with the 45° bend, the flow changes direction more smoothly. In the channel with the 90° bend, a sharper redistribution of velocity is observed in the bend region. The maximum velocity values are mainly located in the central part of the channel, while near the walls the velocity decreases because of the no-slip condition. A feature of this result is that, under the same computational conditions, the channel with the 45° bend gives a more uniform flow motion than the 90° channel. This is explained by the fact that, at the angle of 45°, the change in the direction of motion occurs gradually, while at the angle of 90° the flow has to change direction sharply.

2. The pressure distribution in channels with bend angles of 45° and 90° was analyzed. It was found that, for all considered Reynolds numbers, the pressure is higher in the inlet region and decreases toward the outlet. At the same time, the pressure drop in the channel with the 90° bend is larger than in the channel with the 45° bend. According to the results of comparison of hydrodynamic flow characteristics in channels with bend angles of 45° and 90° at different configurations, at Re = 500, the value of ΔP is 0.260596 for the 45° channel and 0.286797 for the 90° channel; at Re = 1000, the values are 0.123542 and 0.136875, respectively; at Re = 2000, the values are 0.055111 and 0.061812, respectively. Therefore, the sharp 90° bend causes larger pressure losses. In contrast to the smoother 45° bend, the 90° geometry creates stronger resistance to the flow because of the sharp change in the direction of motion.

3. The behavior of the stream function was studied for Reynolds numbers Re = 500, 1000, and 2000. In the channel with the 45° bend, the stream-function lines are distributed rather uniformly for all considered values of Re. This shows that the flow structure remains stable and smooth even when the Reynolds number increases. In the channel with the 90° bend, vortex zones appear after the bend as Re increases. This is especially visible at Re = 1000 and Re = 2000. This result differs from the 45° case, where clear vortex formation is not observed. The appearance of vortex zones in the 90° channel is explained by the fact that the flow does not have enough space to rearrange smoothly after the sharp bend.

4. A quantitative comparison of hydrodynamic characteristics for the two channel geometries was carried out. According to modeling results, the values of the resistance coefficient C_f and the Euler number Eu are higher for the channel with the 90° bend in all cases. For example, at Re = 500, the coefficient C_f is 0.5212 for the 45° channel and 0.5736 for the 90° channel; at Re = 2000, the values are 0.1102 and 0.1236, respectively. A similar pattern is observed for the Euler number Eu. This confirms that the channel with the 90° bend gives greater hydrodynamic resistance to the flow. Compared with known approaches to the analysis of flows in channels with complex geometry, the present work gives a direct comparison of two bend angles under the same computational parameters. This makes it possible to show more clearly the influence of the channel geometry itself.

Conflict of interest

The authors declare that they have no conflicts of interest in connection with this study, including financial, personal, authorial, or any other that might affect the study and results presented in this paper.

Financing

This study is funded by the Science Committee of the Ministry of Science and Higher Education of the Republic of Kazakhstan (Grant No. AP22688601).

Data availability

Manuscript has no associated data.

Use of artificial intelligence

During the preparation of this manuscript, the authors used ChatGPT, model GPT-5.5, only for language-level checking of the manuscript text. The tool was used to check grammar, spelling, and punctuation in the following sections: Abstract, Introduction, Literature review and problem statement, The aim and objectives of the study, Materials and methods, Numerical results of modeling the flow in bended channels, Discussion of the results of modeling, Conclusion.

The AI tool was not used to generate research ideas, formulate the hypothesis, develop the methodology, write or rewrite substantive parts of the manuscript, generate or analyze data, create conclusions, create figures, or generate code. No scientific content, numerical results, interpretation of results, references, or conclusions were produced by the AI tool.

After using the tool, the authors checked all suggested corrections manually and compared the edited text with the

original manuscript. Only language corrections that did not change the scientific meaning, mathematical formulations, numerical data, interpretation of results, or conclusions were accepted. The authors take full responsibility for the final content of the manuscript.

The use of the AI tool did not influence the results, discussion, or conclusions of the study; it affected only the correction of grammar, spelling, and punctuation.

Authors' contributions

Almas Temirbekov: Software, Resources, Data Curation; **Zhadra Zhaksylykova:** Methodology, Formal analysis, Investigation, Writing-original draft, Writing-review & editing, Project administration, Funding acquisition; **Bekdaulet Khudaibergen:** Validation, Visualization, Resources; **Nurlan Temirbekov:** Conceptualization, Supervision, Formal analysis.

References

1. Glowinski, R. (1984). Numerical Methods for Nonlinear Variational Problems. Springer Berlin Heidelberg. https://doi.org/10.1007/978-3-662-12613-4
2. Olshanskii, M. A. (2002). A low order Galerkin finite element method for the Navier–Stokes equations of steady incompressible flow: a stabilization issue and iterative methods. Computer Methods in Applied Mechanics and Engineering, 191 (47-48), 5515–5536. https://doi.org/10.1016/s0045-7825(02)00513-3
3. Varun Kumar, R., Nagaraja, K. V., Kovács, E., Shah, N. A., Chung, J., Prasannakumara, B. C. (2023). Accelerating finite element modeling of heat sinks with parallel processing using FEniCSx. Case Studies in Thermal Engineering, 44, 102865. https://doi.org/10.1016/j.csite.2023.102865
4. Larson, M. G., Bengzon, F. (2013). The Finite Element Method: Theory, Implementation, and Applications. Springer Berlin Heidelberg. https://doi.org/10.1007/978-3-642-33287-6
5. Zienkiewicz, O. C., Taylor, R. L., Zhu, J. Z. (2013). The Finite Element Method: Its Basis and Fundamentals. Oxford: Butterworth-Heinemann. https://doi.org/10.1016/c2009-0-24909-9
6. Bilal, F. S., Sedrez, T. A., Shirazi, S. A. (2021). Experimental and CFD investigations of 45 and 90 degrees bends and various elbow curvature radii effects on solid particle erosion. Wear, 476, 203646. https://doi.org/10.1016/j.wear.2021.203646
7. Ben Haroual, B., Albagnac, J., Brancher, P., Cazin, S., Boldo, D., Thibert, E., Mathis, R. (2025). Experimental investigation of Dean-vortices oscillation downstream of a 90° Bend. Experimental Thermal and Fluid Science, 163, 111402. https://doi.org/10.1016/j.expthermflusci.2024.111402
8. Heskestad, G. (1971). Two-Dimensional Miter-Bend Flow. Journal of Basic Engineering, 93 (3), 433–443. https://doi.org/10.1115/1.3425271
9. Yamashita, H., Izumi, R., Kushida, G., Mizuno, T. (1986). Fluid Flow and Heat Transfer in a Two-dimensional Miter-bend : 1st Report, Experiments and Analyses. Bulletin of JSME, 29 (258), 4164–4169. https://doi.org/10.1299/jsme1958.29.4164
10. Xiong, R., Chung, J. N. (2008). Effects of miter bend on pressure drop and flow structure in micro-fluidic channels. International Journal of Heat and Mass Transfer, 51 (11-12), 2914–2924. https://doi.org/10.1016/j.ijheatmasstransfer.2007.09.018
11. Al-Tameemi, W. T. M., Ricco, P. (2018). Pressure-Loss Coefficient of 90 deg Sharp-Angled Miter Elbows. Journal of Fluids Engineering, 140 (6). https://doi.org/10.1115/1.4038986
12. Villegas-León, J. J. (2025). Head losses and experimental loss coefficient in 45° and 90° elbow of pvc small-diameter pipes for single-phase flow and moderate reynolds numbers. Journal of Southwest Jiaotong University, 3. https://doi.org/10.35741/issn.0258-2724.60.3.5
13. Varun Kumar, R., Nagaraja, K. V. (2023). Steady solver for incompressible Navier-Stokes equation with automated adaptive mesh refinement using FEniCS. Materials Today: Proceedings. https://doi.org/10.1016/j.matpr.2023.04.425
14. Temirbekov, A., Baigereyev, D., Temirbekov, N., Urmashev, B., Amantayeva, A. (2021). Parallel CUDA implementation of a numerical algorithm for solving the Navier-Stokes equations using the pressure uniqueness condition. International Conference on Analysis and Applied Mathematics (Icaam 2020), 2325, 20063. https://doi.org/10.1063/5.0041039
15. Temirbekov, A., Altybay, A., Temirbekova, L., Kasenov, S. (2022). Development of parallel implementation for the Navier-Stokes equation in doubly connected areas using the fictitious domain method. Eastern-European Journal of Enterprise Technologies, 2 (4 (116)), 38–46. https://doi.org/10.15587/1729-4061.2022.254261
16. Temirbekov, A., Zhaksylykova, Z., Malgazhdarov, Y., Kasenov, S. (2022). Application of the Fictitious Domain Method for Navier-Stokes Equations. Computers, Materials & Continua, 73 (1), 2035–2055. https://doi.org/10.32604/cmc.2022.027830
17. Baitulenov, Z., Olshanskii, M., Temirbekov, A., Temirbekov, N., Kasenov, S. (2026). A Modified Brinkman Penalization Fictitious Domain Method for the Unsteady Navier-Stokes Equations. Numerical Methods for Partial Differential Equations, 42 (3). https://doi.org/10.1002/num.70089
18. Temirbekov, N., Khakimzyanov, G., Kerimakyn, A. (2026). Application of the Curvilinear Coordinate Method for the Numerical Solution of the Navier–Stokes Equations in Domains with Complex Boundaries. Computation, 14 (3), 58. https://doi.org/10.3390/computation14030058

19. Çengel, Y., Cimbala, J. (2017). Fluid Mechanics: Fundamentals and Applications. New York: McGraw-Hill Higher Education, 1024.
20. Galdi, G. P. (2011). An Introduction to the Mathematical Theory of the Navier-Stokes Equations. Springer Monographs in Mathematics. Springer New York. https://doi.org/10.1007/978-0-387-09620-9
21. Automated Solution of Differential Equations by the Finite Element Method (2012). Lecture Notes in Computational Science and Engineering. Springer Berlin Heidelberg. https://doi.org/10.1007/978-3-642-23099-8
22. Langtangen, H. P., Mardal, K.-A. (2016). Introduction to Numerical Methods for Variational Problems. Available at: http://hplgit.github.io/fem-book/doc/web/
23. Alnæs, M. S., Blechta, J., Hake, J. et al. (2015) The FEniCS Project Version 1.5. Archive of Numerical Software, 3 (100), 23. https://doi.org/10.11588/ans.2015.100.20553
24. Langtangen, H. P., Logg, A. (2016). Solving PDEs in Python. Springer International Publishing. https://doi.org/10.1007/978-3-319-52462-7
25. Kumar, V., Chandan, K., Nagaraja, K. V., Reddy, M. V. (2022). Heat Conduction with Krylov Subspace Method Using FEniCSx. Energies, 15 (21), 8077. https://doi.org/10.3390/en15218077
26. Geuzaine, C., Remacle, J.-F. (2009). Gmsh: A 3-D finite element mesh generator with built-in pre- and post-processing facilities. International Journal for Numerical Methods in Engineering, 79 (11), 1309–1331. https://doi.org/10.1002/nme.2579
27. Baigereyev, D., Omariyeva, D., Temirbekov, N., Yergaliyev, Y., Boranbek, K. (2022). Numerical Method for a Filtration Model Involving a Nonlinear Partial Integro-Differential Equation. Mathematics, 10 (8), 1319. https://doi.org/10.3390/math10081319